Title

Time Course of Pathogenic and Adaptation Mechanisms in Cystinotic Mouse Kidneys

Journal

Journal of the American Society of Nephrology, 25(6)

ISSN

1046-6673

Authors

Gaide Chevronnay, Héloïse P
Janssens, Virginie
Van Der Smissen, Patrick
et al.

Publication Date

2014-06-01

DOI

10.1681/asn.2013060598

Peer reviewed

BASIC RESEARCH www.jasn.org

Time Course of Pathogenic and Adaptation Mechanisms in Cystinotic Mouse Kidneys

Héloïse P. Gaide Chevronnay,* Virginie Janssens,* Patrick Van Der Smissen,* Francisca N'Kuli,* Nathalie Nevo,† Yves Guiot,‡ Elena Levtchenko,§ Etienne Marbaix,*‡ Christophe E. Pierreux,* Stéphanie Cherqui,‖ Corinne Antignac,† and Pierre J. Courtoy*

*Cell Biology Unit, de Duve Institute and Université Catholique de Louvain, Brussels, Belgium; †Inserm, U574, Hôpital Necker-Enfants Malades and Université Paris Descartes, Sorbonne Paris Cité, Institut Imagine, Paris, France; ‡Pathology Department, Saint-Luc University Clinics, Brussels, Belgium; §Department of Pediatric Nephrology, University Hospitals Leuven, Leuven, Belgium; and ‖Department of Pediatrics, Division of Genetics, University of California, San Diego, California

ABSTRACT

Cystinosis, a main cause of Fanconi syndrome, is reproduced in congenic C57BL/6 cystinosin knockout (KO) mice. To identify the sequence of pathogenic and adaptation mechanisms of nephropathic cystinosis, we defined the onset of Fanconi syndrome in KO mice between 3 and 6 months of age and analyzed the correlation with structural and functional changes in proximal tubular cells (PTCs), with focus on endocytosis of ultrafiltrated disulfide-rich proteins as a key source of cystine. Despite considerable variation between mice at the same age, typical event sequences were delineated. At the cellular level, amorphous lysosomal inclusions preceded cystine crystals and eventual atrophy without crystals. At the nephron level, lesions started at the glomerulotubular junction and then extended distally. *In situ* hybridization and immunofluorescence revealed progressive loss of expression of megalin, cubilin, sodium-glucose cotransporter 2, and type IIa sodium-dependent phosphate cotransporter, suggesting apical dedifferentiation accounting for Fanconi syndrome before atrophy. Injection of labeled proteins revealed that defective endocytosis in S1 PTCs led to partial compensatory uptake by S3 PTCs, suggesting displacement of endocytic load and injury by disulfide-rich cargo. Increased PTC apoptosis allowed luminal shedding of cystine crystals and was partially compensated for by tubular proliferation. We conclude that lysosomal storage triggered by soluble cystine accumulation induces apical PTC dedifferentiation, which causes transfer of the harmful load of disulfide-rich proteins to more distal cells, possibly explaining longitudinal progression of swan-neck lesions. Furthermore, our results suggest that subsequent adaptation mechanisms include lysosomal clearance of free and crystalline cystine into urine and ongoing tissue repair.

J Am Soc Nephrol 25: ●●●–●●●, 2014. doi: 10.1681/ASN.2013060598

Infantile cystinosis, a multisystemic lysosomal thesaurismosis, causes renal Fanconi syndrome in the first year of life and kidney failure after a decade, even under compliant cysteamine therapy.[1,2] Lysosomal cystine accumulation and precipitation into crystals result from defective export caused by lack of the H^+: cystine membrane symporter, cystinosin (*CTNS*).[3,4] Nephropathic cystinosis is reproduced in congenic $Ctns^{-/-}$ C57BL/6 mice,[5] but strong dependence of genetic background suggests complex disease mechanisms and important modifier genes.

In cystinotic neutrophils, cystine accumulates in lysosomes without changing their equilibrium density, despite high gravity of cystine crystals,

Received June 10, 2013. Accepted November 15, 2013.

Published online ahead of print. Publication date available at www.jasn.org.

Correspondence: Dr. Héloïse P. Gaide Chevronnay, de Duve Institute and Université Catholique de Louvain, 75, Avenue Hippocrate, PO Box B1.75.05, 1200 Brussels, Belgium. Email: heloise.gaidechevronnay@uclouvain.be

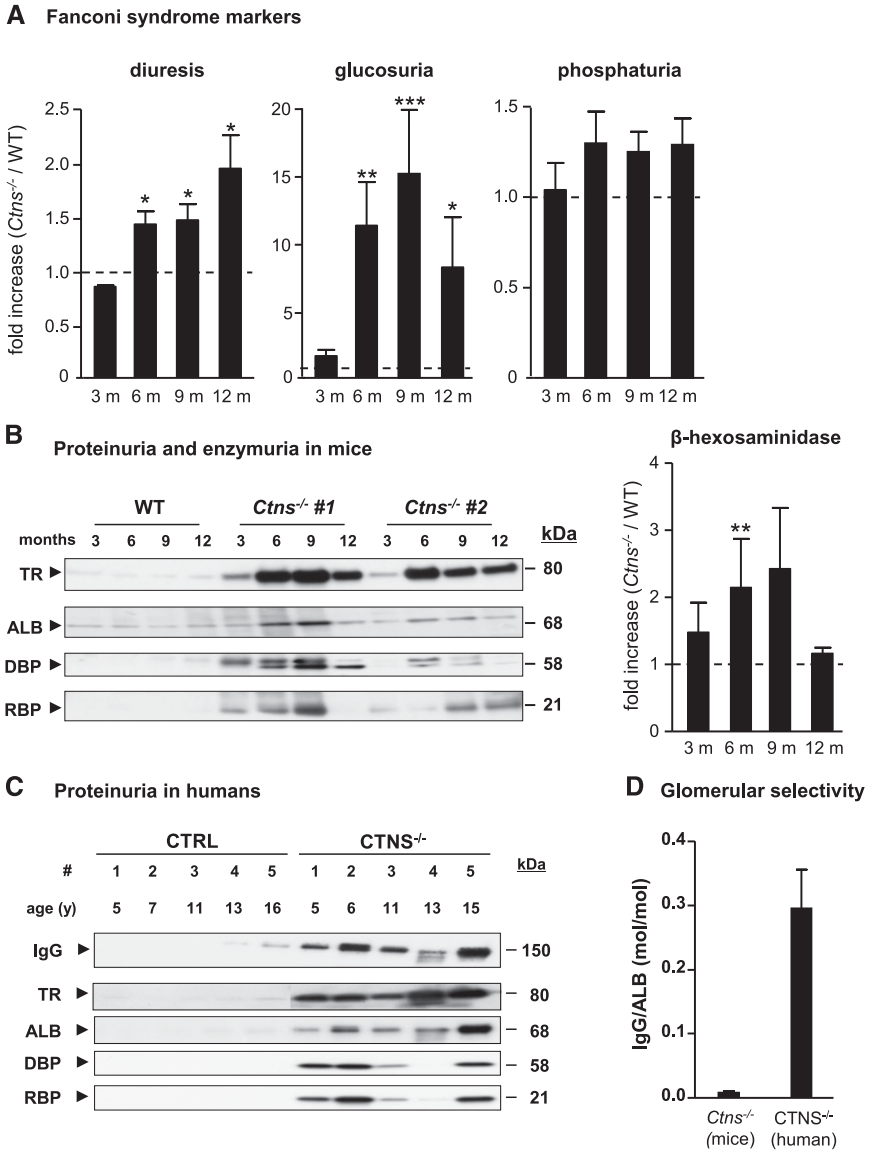

Figure 1. *Ctns*$^{-/-}$ mice develop a partial Fanconi syndrome between 3 and 6 months. Twenty-four–hour urine collections were obtained on ice with protease inhibitors from 3-, 6-, 9-, and 12-month-old C57BL/6 WT and *Ctns*$^{-/-}$ mice (n=8 for each interval). (A) Time course of the loss of solutes in *Ctns*$^{-/-}$ mice. Volume, glucose, and phosphate excretion were normalized to control values in age-matched WT mice. (B) Time course of proteinuria and enzymuria in *Ctns*$^{-/-}$ mice. Representative Western blots for transferrin (TR), albumin (ALB), vitamin D binding protein (DBP), and RBP in one WT and two *Ctns*$^{-/-}$ mice (#1 and #2) in serial collections at the indicated ages (loads normalized to 2 μg creatinine). Blots were processed strictly in parallel. *N*-Acetyl-β-hexosaminidase activity (a representative lysosomal hydrolase[49] insensitive to protease inhibitors) was normalized to control values in age-matched WT mice (there was no detectable change in its mRNA; not shown). Notice the consistent increase of solutes and most tested proteins between 3 and 6 months. *P<0.05; **P<0.01; ***P<0.001. Supplemental Figure 1 shows quantitation of individual proteinuria in all time course collections. (C) Urinalysis by Western blotting in five cystinotic children versus five age-matched controls. Loads were normalized to 2 μg creatinine like in B, and blots were processed strictly in parallel. Note the strong detection of IgG, TR, and ALB in all patients as well as DBP and RBP, except in outlier patient 4 without Fanconi syndrome. CTRL, control. (D) Glomerular selectivity in cystinotic mice but not patients. Normalized urinary loads of five cystinotic children and 3- to 9-month-old mice were analyzed by Western blotting for IgG and ALB by reference to increasing standards of fresh plasma in the same blots. Data are presented as mean±SEM of IgG/ALB molar ratios in cystinotic mice (*Ctns*$^{-/-}$) compared with cystinotic children (CTNS$^{-/-}$).

indicating predominant accumulation in noncrystalline form.[6] Furthermore, by electron microscopy, enlarged acid–phosphatase-labeled structures enclose an amorphous matrix without systematic association with crystals.[7] Cystinotic fibroblasts show enlarged lysosomes without acidification defect[8] and accumulate cystine on degradation of endocytosed disulfide-rich proteins, such as albumin, in proportion to extracellular concentration.[9–12] However, retention is surprisingly low (approximately 1%), possibly because of vesicular exodus.[10,11] Exodus is linked to endocytic recycling,[10–12] which involves tiny tubular endosomes (thus size-limited) and is particularly active in kidney proximal tubular cells (PTCs).[13,14] These observations indicate potent lysosomal discharge, now a recognized common feature of lysosomal storage diseases.[15]

Although the genetic and cellular bases of cystinosis are clear, little is known on (*1*) the early structural and molecular changes in the complex kidney architecture leading to the Fanconi syndrome, (*2*) their significance for cystinosis progression along uriniferous nephron (reviewed in ref.[16]), (*3*) the pathogenic role of cystine crystals, and (*4*) natural adaptation mechanisms. In cystinotic kidneys, Fanconi syndrome is generally attributed to PTC atrophy, starting at the glomerulotubular junction as swan-neck deformities, but earlier functional defects caused by impaired gene expression were not considered.[17] However, as shown in polarized PTCs cultures, expression of apical endocytic receptors strongly depends on differentiation state.[18]

To address these issues, we exploited congenic *Ctns*$^{-/-}$ C57BL/6 mice,[5] which allowed us to study early kidney events that are inaccessible in patients. This established model shows (*1*) high cystine levels,

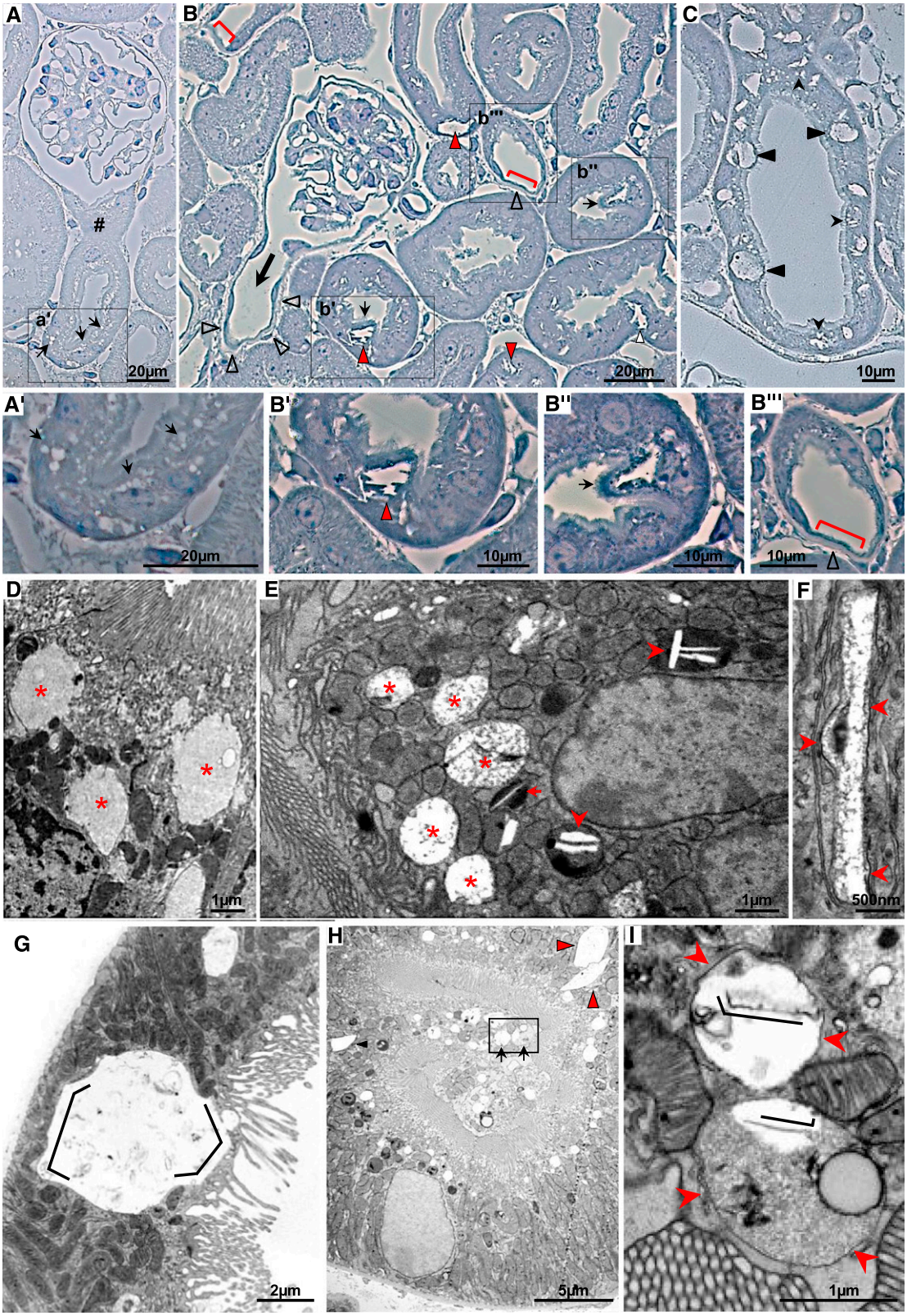

Figure 2. Kidney lesions in cystinotic mice start in S1 proximal tubular cells by apical vacuolation due to amorphous inclusions, which slowly convert into membrane-bound crystals of increasing size. Overview of (A–C) histologic (semithin plastic sections) and (D–I) ultrastructural alterations of *Ctns*$^{-/-}$ mice kidneys. (A) In this representative 6-month sample, notice the early apical vacuolation (small arrows; box is enlarged in A') limited to proximal PTCs at the glomerulotubular junction (#), contrasting with the apparent integrity of all other kidney tissues. (B) In this

including kidney crystals, (*2*) renal lesions with Fanconi syndrome, and (*3*) progression to kidney failure. The aim of our study was to bridge the gaps between cell biologic studies addressing short-term events in cultures of short-lived or rapidly dividing cells and a chronic disease affecting highly differentiated quiescent cells in a complex tubular organ.

To investigate the physiopathology of nephropathic cystinosis progression, we took the perspective of endocytic uptake of ultrafiltrated plasma proteins as an essential cystine source. Disulfide bonds are abundant in plasma proteins (17/albumin) but virtually absent in cytosolic and mitochondrial proteins.[19] In normal human PTCs, daily endocytic reuptake of approximately 7 g albumin[20] is, thus, a major source of lysosomal cystine, far above autophagy.[21] PTCs are specialized to capture ultrafiltrated proteins by apical receptor-mediated endocytosis (ARME) through abundantly expressed, rapidly recycling multiligand tandem receptors, megalin, and cubilin.[22] Megalin- and cubilin-knockout mice show defective PTC endocytosis and urinary loss of ultrafitrated plasma proteins[23–26] and lysosomal enzymes.[27,28] Although defective ARME caused by loss of megalin/cubilin was a possible explanation for proteinuria of cystinotic patients, normal immunolabeling of megalin/cubilin was reported in an end stage cystinotic kidney despite massive proteinuria, calling attention to glomerular leakage.[29]

Ctns$^{-/-}$ mice allowed us to (*1*) identify sequential changes in the form of lysosomal storage, (*2*) distinguish dedifferentiation (including megalin and cubilin loss) from atrophy, and (*3*) identify adaptation mechanisms by cystine discharge (including apoptosis shedding) and proliferative epithelial repair.

RESULTS

A Latent Phase Precedes Renal Fanconi Syndrome in *Ctns*$^{-/-}$ Mice

Ctns$^{-/-}$ mice aged 2–9 months show clinical Fanconi syndrome.[5] To better define the disease time course, we first monitored 24-hour urine collections sampled every 3 months for loss of water, glucose, phosphate, and proteins as renal Fanconi syndrome markers (Figure 1A, Supplemental Figure 1). All rose between 3 and 6 months and further increased at 9–12 months, with major individual variation at given ages despite high congenicity. Proteinuria included albumin, transferrin, vitamin D binding protein, retinol binding protein (RBP), and the very sensitive marker CC16 (250-fold at 12 months). These kinetics resembled early Fanconi syndrome of human nephropathic cystinosis. Negligible IgG loss (IgG/albumin molar ratio=1:100) indicated pure PTC dysfunction (without glomerular leakage). Careful blot inspection in serial collections disclosed asynchronous protein loss (*e.g.*, earlier increase of the cubilin ligand, transferrin, and later megalin ligand, RBP) (Figure 1B). Increased urinary β-hexosaminidase (despite comparable gene expression; not shown) was compatible with defective reuptake of ultrafiltrated lysosomal enzymes. Four cystinotic children aged 5–15 years old with renal Fanconi syndrome also exhibited strong urinary excretion of transferrin, albumin, vitamin D binding protein, and RBP, which was not detected in control samples (Figure 1C), but high IgG/albumin loss (0.3), indicating concomitant glomerular leakage.

Integrated Sequence of Histologic and Lysosomal Changes

Histologic lesions started at approximately 6 months in superficial cortex (Supplemental Figure 2), thus possibly first affecting superficial nephrons,[30] in PTCs next to the glomerulotubular junction (S1) (Figure 2A) and then extended deeper with considerable heterogeneity: typical patterns will, thus, be described. At the cellular level, we first noted apical swelling (Figure 2, A and A′), which corresponded to amorphous inclusions of increasing electron density (Figure 2, D and E) (like in human cystinotic leukocytes) distinct from electron lucent endosomes and more basally located dense bodies. Lysosomal nature of inclusions was confirmed by LAMP-1 immunofluorescence (as the lysosomal membrane marker) and filling with injected horseradish peroxidase (HRP) as a classic endocytic tracer[31] (Figure 3).

representative 9-month sample, PTCs at the glomerulotubular junction have been replaced by a flat epithelium, indistinguishable from Bowman's capsule (thick arrow) and likewise resting on a thick basement membrane (open arrowheads). Crystals are obvious in several other PTCs (red arrowheads), which are better seen in the boxes enlarged in B′ and B″. Arrows points to apical bulging. Brackets delineate individual cell flattening (enlarged at B″′). (C) In this representative 12-month sample, numerous PTCs with preserved height and visible brush border contain collections of small crystals (small arrowheads) or enclose a large vacuole (large arrowheads). (D) This ultrastructural view of the apical region of a *Ctns*$^{-/-}$ PTC at 6 months shows well differentiated brush border and three large inclusions with amorphous content (asterisks). (E) In this 12-month sample, notice the apparent progression of the changes from vacuolation and amorphous inclusion (asterisks) up to dense bodies of normal size harboring small crystals (thin needle at small arrow; thicker crystals at arrowheads). In two other 12-month samples, notice (F) a single membrane-bound (arrowheads) crystal (3-μm long and 200-nm thick) with a fine electron-dense fibrillar matrix and (G) a large vacuole with straight membrane border segments connected at rigid angles (polygonal lines) indicating deformation by packed cystine crystals. This vacuolar expansion almost spans the entire cell height, except for its most basal cytoplasm resting on a nondistorted basement membrane, and causes luminal bulging of the apical surface, which still bears numerous microvilli. (H) In this other 12-month sample (box enlarged in I), largely preserved PTCs (except for a few crystals; arrowheads) surround a lumen enclosing cell debris, including a membrane-bound lysosome (delineated by arrowheads) containing two crystals (polygonal lines).

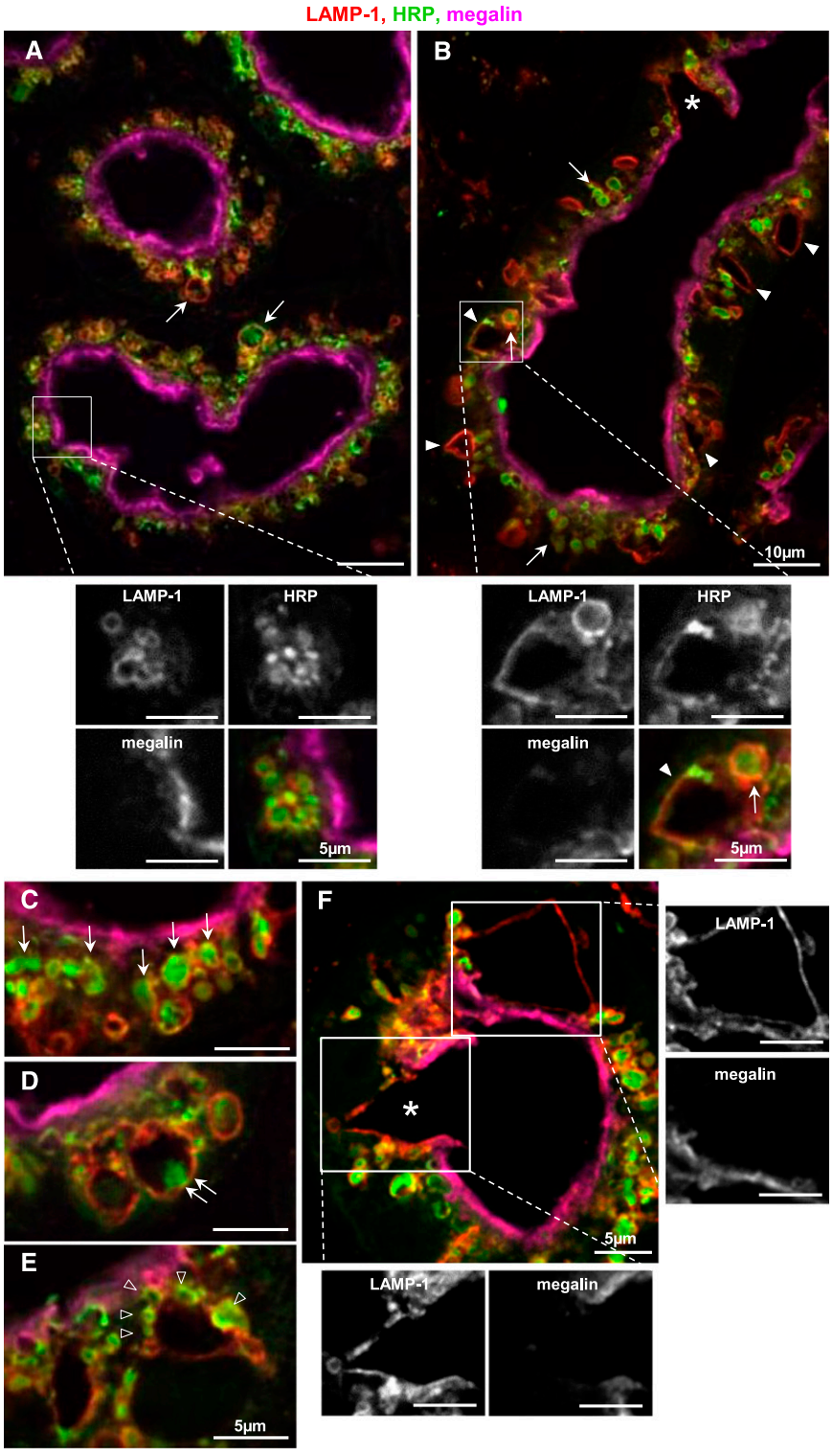

Figure 3. Triple immunofluorescence identifies enlarged vacuoles and crystal-bearing structures as lysosomes, which progressively disconnect from active endocytic trafficking (residual bodies) and can discharge their content into the tubular lumen (lysosomal defecation). Comparison of (A) WT and (B–F) *Ctns*$^{-/-}$ mice for labeling of megalin (magenta) to identify PTCs, LAMP-1 (red) to label the lysosomal membrane, and HRP injected 2 hours before euthanization (green) to test for lysosomal accessibility and matrix filling. In enlarged boxed fields, individual antigens are presented in black and white for optimal resolution and easier pattern comparison as well as merged triple colors. (A) Control. In this 6-month WT mouse kidney, PTCs show homogenous-intense (sub)apical labeling for megalin at the expected position for the base of brush border and endosomes; most lysosomes are clustered and exhibit uniformly round shape, similar size, and extensive filling by HRP. The two short arrows point to very rare enlarged lysosomes. (B–F) *Ctns*$^{-/-}$. In this 6.5-month sample with unusually advanced lesions, notice that most PTCs show (*1*) alterations of LAMP-1–labeled lysosomes, including round expansion with preserved HRP filling (arrows in B and C) or only partial HRP filling (double arrows in D); (*2*) spindle-shaped deformation with progressive loss of accessibility to the endocytic tracer (filled arrowheads in B); (*3*) extensive spindle-shaped or ovoid deformations, almost spanning the cell size, with docked but not fused lysosomes[50] (open arrowheads in E); and (*4*) apparent continuity of LAMP-1 (red) with strong apical megalin labeling (magenta) at adjacent cells (asterisks at B and F; enlarged below). The other field enlarged at right shows a huge lysosome (>10 μm) with straight borders at a rigid angle (upper enlargement) that is resolved from a dense apical megalin signal. It is not possible to distinguish whether these two objects belong to the same or overlapping cells.

Because cystine crystals dissolve on section rehydratation, they were identified as characteristic light and electron lucent needles and then, micrometers-long polyhedric objects enclosed by a limiting membrane. As lesions progressed, we noted crystal buildup in cells with preserved height and microvilli (Figure 2B) and then, coalescence into huge and distorted single vacuoles up to luminal bulging (Figure 2, B′, B″, and C). Vacuoles were still labeled for LAMP-1 but progressively lost accessibility to HRP (Figure 3). Coalescent cystine crystals imposed characteristic polygonal membrane deformation that were visible by electron (Figure 2G) and even light microscopy (Figure 3, B–F). LAMP-1 immunofluorescence revealed occasional cavities within proximal epithelium that were open to lumen, showing apparent continuity between lateral LAMP-1 and apical megalin (of adjacent cells?) and

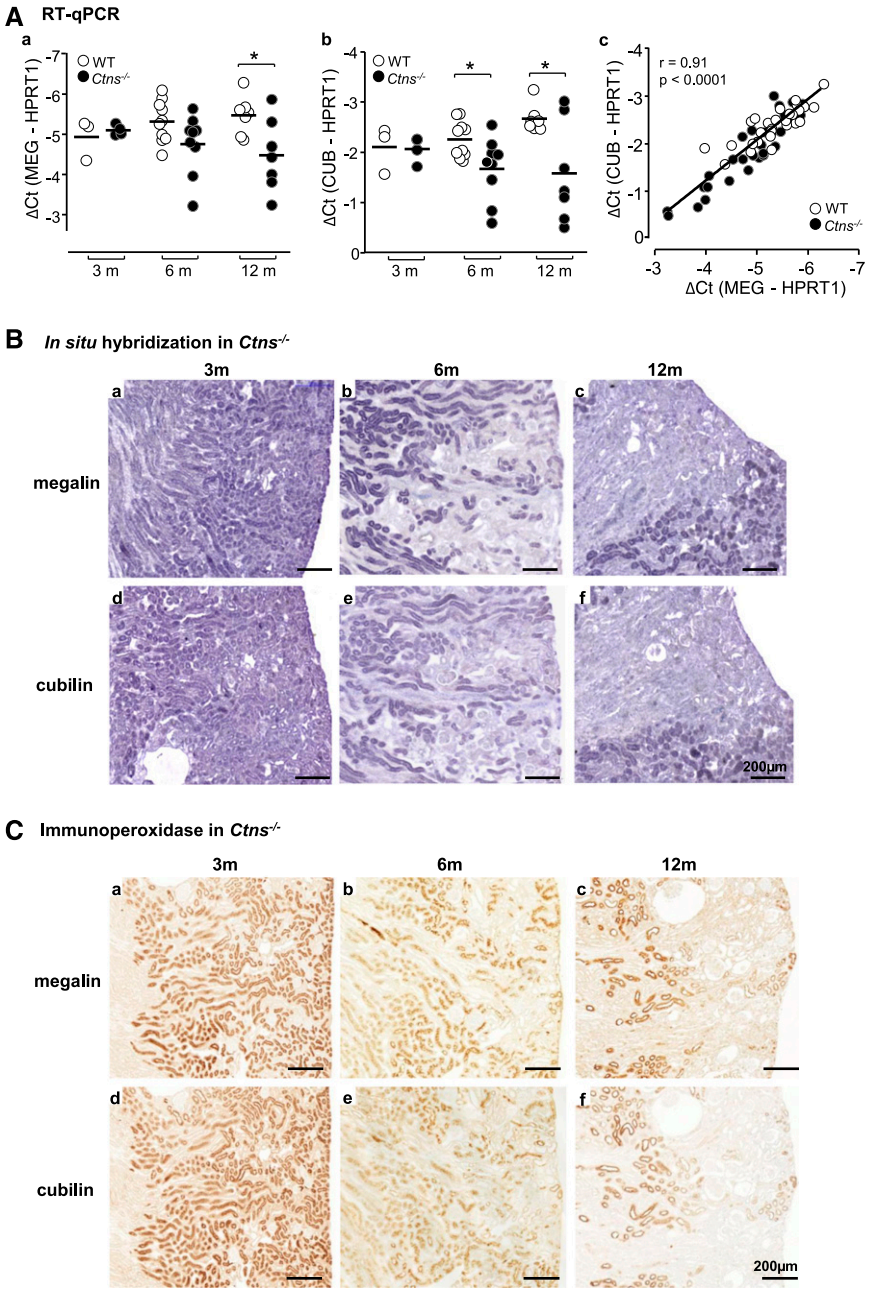

Figure 4. Proximal tubular cells show progressive loss of megalin and cubilin mRNA and protein expression. (A) Quantification by quantitative RT-PCR (RT-qPCR) of (a) megalin (MEG) and (b) cubilin (CUB) mRNAs in WT and *Ctns*$^{-/-}$ kidneys collected at 3, 6, and 12 months normalized to hypoxanthine phosphoribosyltransferase-1 (HPRT1) and presented as ΔCt values. *$P<0.05$. (c) Robust correlation over a 10-fold range between MEG and CUB mRNA expression levels suggests common transcriptional regulation[18] modulated by variations of local cellular insult (cystine load). Supplemental Figure 2 shows preservation of global mRNA expression of glomerular (podocin) and distal nephron markers (sodium–glucose cotransporter-1 [SGLT-1] and aquaporin-2 [AQP-2]) in *Ctns*$^{-/-}$ kidneys. (B and C) Localization by (B) *in situ* hybridization and (C) immunoperoxidase of (a–c) megalin and (d–f) cubilin in *Ctns*$^{-/-}$ mice kidney paraffin sections at (a and d) 3, (b and e) 6, and (c and f) 12 months. Scale bars, 200 μm. Notice progressive extinction of the expression of both receptors from the superficial cortex into deeper zones. Supplemental Figure 4 shows half-kidney sagittal images. Supplemental Figure 5 shows quantification of loss of megalin and cubilin proteins in kidney homogenates by Western blotting.

suggesting fusion of crystal-loaded residual bodies with apical membrane (*i.e.*, luminal exocytosis by living cells) (Figure 3F). Alternatively, apoptotic fragments were shed in lumen, some bearing recognizable crystals (Figure 2, H and I). Shedding caused piecemeal flattening (Figure 2B), sharply alternating with preserved cells. At 9–12 months, all tubular cells close to glomerulotubular junction in affected nephrons became extremely flat, indistinguishable from Bowman's epithelium, and likewise, rested on very thick basement membrane (Figure 2B). All other kidney cells remained unaltered, arguing against uniform cystine production from endogenous proteins. Up to 9 months, glomeruli appeared essentially intact (not shown), but at 12 months, dilated renal corpuscles with enlarged Bowman's space and collapsed capillary tufts, compatible with glomerulotubular disconnection, became obvious.

Altogether, these data showed selective distally extending PTC lesions, with a sequence of lysosomal lesions involving (*1*) amorphous inclusions, (*2*) crystallization into small needles within typical dense bodies, (*3*) larger membrane-bound crystals in residual bodies progressively excluded from endocytic trafficking, (*4*) huge crystal collections in single distorted lysosomal vacuoles, (*5*) luminal discharge by apical fusion or shedding as apoptotic bodies, and (*6*) absence of crystal in established swan-neck lesions.

Defective Megalin and Cubilin Expression in *Ctns*$^{-/-}$ Mice Kidneys

Because urinary loss of ultrafiltrated plasma proteins suggested defective ARME, we next analyzed endocytic receptors expression at mRNA and protein levels. By quantitative RT-PCR (Figure 4A) and Western blotting (Supplemental Figure 5) on total extracts, megalin and cubilin decreased from 6 to 12 months in *Ctns*$^{-/-}$ mice, with high variation between individuals at given ages but strong correlation of megalin versus cubilin mRNAs or proteins within individuals (over 1 log). In contrast, neither podocin (glomeruli) nor sodium–glucose transporter-1 (SGLT-1) (straight segment) and aquaporin-2 (collecting duct) expression was significantly altered, confirming lesion selectivity to PTCs

(Supplemental Figure 3B). By *in situ* hybridization and immunoperoxidase, megalin and cubilin mRNA and protein were homogenously distributed in PTCs of wild-type (WT; not shown) and *Ctns*$^{-/-}$ mice at 3 months (Figure 4, B and C). We noticed complete loss of megalin and cubilin expression in superficial foci of *Ctns*$^{-/-}$ cortex at 6 months, extending at 12 months into the outer medulla (Figure 4, B and C) and matching extension of histologic lesions (large fields at Supplemental Figure 4).

Cystinotic Patients Also Show Defective Megalin and Cubilin Expression Associated with Proteinuria

Preservation of megalin/cubilin had, however, been reported in a cystinostic child kidney biopsy.[29] We, thus, reinvestigated megalin/cubilin expression in kidney paraffin blocks archived from a 3-year-old cystinotic child, an age-matched control with preserved renal function, and four older cystinotic children with kidney dysfunction (Supplemental Table 3). In the 3-year-old cystinotic kidney, most PTCs exhibited strong megalin/cubilin immunostaining, which lacked in adjacent atrophic PTCs (Figure 5, B and E, arrowheads). In contrast, all samples from older patients, including the case previously reported,[29] showed only rare foci of PTCs retaining strong megalin/cubilin signal among profoundly disorganized tissue lacking endocytic receptors (Figure 5, C and F). Thus, cystinotic mouse and human kidneys exhibited similar tissue heterogeneity with progressive loss of megalin/cubilin.

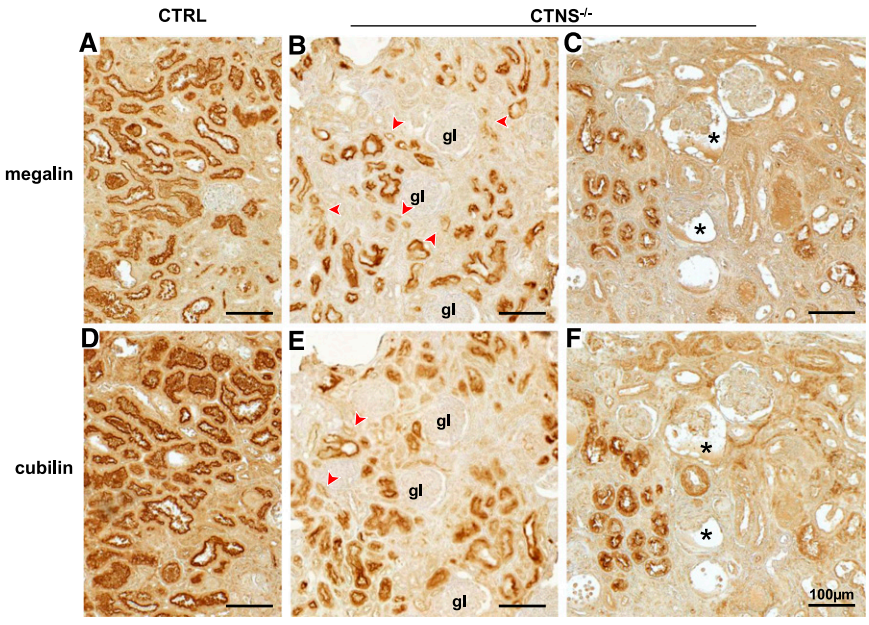

Figure 5. Cystinotic children also show progressive loss of megalin and cubilin in kidney proximal tubules. Immunoperoxidase of (A–C) megalin and (D–F) cubilin on adjacent kidney paraffin sections from (A and D) a control child biopsy (3-year-old child with primary oxaluria), (B and E) a 3-year-old cystinotic girl with Fanconi syndrome but normal plasma creatinine value (early case), and (C and F) an 8-year-old cystinotic girl with end stage kidney disease (terminal case; representative of four cases). In the absence of cystinosis, megalin and cubilin label all PTCs uniformly. (B and E) In the early case of infantile cystinosis, sparse foci with partial or complete loss of megalin and cubilin (arrowheads) are detected among tissue with overall preserved structure and megalin/cubilin expression. gl, glomerulus. (C and F) In the representative terminal case of infantile cystinosis, tissue atrophy is extensive, but some nephrons still express megalin and cubilin. Notice also the two glomerular profiles with expanded Bowman's space and collapsed capillary tuft (asterisks), suggestive of glomerulotubular disconnection. Scale bars, 100 μm.

Apical Receptor-Mediated Endocytosis Is Defective in *Ctns*$^{-/-}$ Kidneys and Causes Transfer of Protein Load in the Nephron

To further test whether proteinuria resulted from defective ARME in PTCs, mice were injected with ^{125}I-β_2-microglobulin or TexasRed-ovalbumin as ultrafiltrated tracers. Average total ^{125}I-β_2-microglobulin uptake only marginally decreased in 12-month-old *Ctns*$^{-/-}$ mice (Figure 6A), contrasting with the severity of histologic lesions. This apparent paradox was addressed by ^{125}I-β_2-microglobulin tissue distribution (Figure 6B). Autoradiography grains were restricted to kidney cortex in WT mice from 3 to 12 months[32] and 3-month-old *Ctns*$^{-/-}$ mice but extended into the outer stripe of outer medulla at 12 months, consistent with transfer of ^{125}I-β_2-microglobulin endocytic load to S3 PTCs on defective S1 uptake.

To establish whether defective uptake correlated with loss of endocytic receptors at the cellular level, we next compared uptake of injected TexasRed-ovalbumin with megalin immunofluorescence (Figure 6C). In WT mice, TexasRed-ovalbumin was restricted to megalin-expressing PTCs, with high cortical load and lesser uptake in a minor fraction of S3 PTCs in the outer stripe of outer medulla. As predicted, cortical *Ctns*$^{-/-}$ PTCs without detectable megalin showed no detectable TexasRed-ovalbumin, which now labeled most S3 *Ctns*$^{-/-}$ PTCs. Thus, decreased megalin/cubilin expression in S1 PTCs resulted in transfer of their normal load of ultrafiltrated disulfide-rich proteins to S3 PTCs, suggesting a molecular and tissular mechanistic explanation for disease extension.

Evaluation of Swan-Neck Lesions by Multiphoton Microscopy

To relate the endocytic defect with extension of swan-neck lesions, kidneys of TexasRed-ovalbumin–injected *Ctns*$^{-/-}$ mice were labeled with Lotus tetragonolobus (LT)-lectin as a PTC marker and analyzed by multiphoton microscopy and three-dimensional reconstruction (Figure 7). PTC dedifferentiation (loss of lectin labeling)

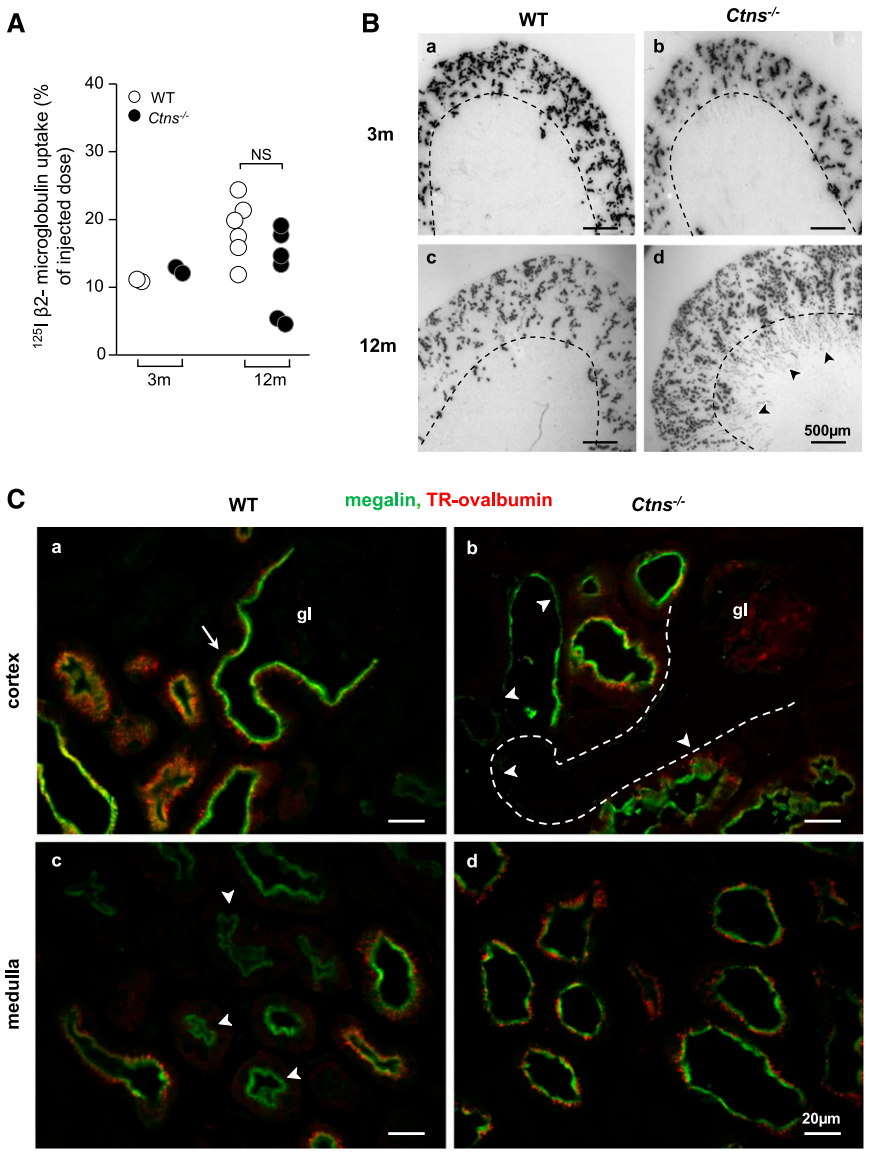

Figure 6. Functional assays by injection of radioiodinated or fluorescent tracers confirm defective apical receptor–mediated endocytosis in affected S1 proximal tubular cells of *Ctns*$^{-/-}$ mice and reveal partial compensatory uptake by S3. (A and B) WT and *Ctns*$^{-/-}$ mice were injected intravenously at 3 or 12 months with ^{125}I-β_2-microglobulin and euthanized after 7 minutes. (A) Quantitation of total uptake in kidney homogenates. Despite strong urinary loss of ultrafiltrated plasma proteins in all *Ctns*$^{-/-}$ mice at 12 months, total renal uptake of ^{125}I-β_2-microglobulin is preserved in most of them. The appoximately 35% average decrease in this cohort is not statistically significant (NS). (B) ^{125}I-β_2-microglobulin localization by autoradiography in representative paraffin kidney sections from (a and b) 3- and (c and d) 12-month-old (a and c) WT and (b and d) *Ctns*$^{-/-}$ mice. Broken lines indicate the corticomedulla boundary. Notice exclusive recapture by cortical PTC segments of control kidneys (a and c) at both intervals and (b) by *Ctns*$^{-/-}$ kidneys at 3 months. (d) In 12-month-old *Ctns*$^{-/-}$ mice, extensive additional distal uptake in PTC of the outer stripe of the outer medulla is indicated by arrowheads. (C) Combination of megalin immunofluorescence with functional study of endocytosis after fluorescent ovalbumin injection. (a and c) WT and (b and d) *Ctns*$^{-/-}$ mice were injected at 9 months with 300 μg TexasRed-ovalbumin (TR-ovalbumin) and euthanized after 20 minutes. Frozen fixed sections were analyzed by double fluorescence microscopy for receptor expression (megalin immunofluorescence is shown by the continuous green apical band) and ligand uptake (ovalbumin is shown by red dots under the megalin layer) in the (a and b) cortex and (c and d) medulla. (a) In WT cortex, notice the strong homogenous double labeling, indicating competence and engagement into ARME by all PTCs in convoluted proximal (cortical) segments, including PTCs at the glomerulotubular junction (arrow). (c) In the WT medulla, tracer uptake is detected in only a fraction of PTCs in the straight segment in the outer stripe of outer medulla, but most S3 profiles are not labeled (arrowheads). (B) In *Ctns*$^{-/-}$ cortex, uptake of TR-ovalbumin is defective in foci of cortical PTCs that have lost megalin (arrowheads), which is best seen at the glomerulotubular junction (contour is indicated by the broken line). (d) In *Ctns*$^{-/-}$ medulla, essentially all S3 PTCs in the outer stripe of outer medulla show preserved megalin expression and are engaged in TR-ovalbumin uptake. This finding suggests partial compensation by S3 uptake in nephrons where ARME is defective in S1 PTCs. Scale bars, 20 μm.

and functional endocytic defect (loss of TexasRed-ovalbumin recapture) could be followed from glomerular junction down to hundreds of micrometers. After abrupt transition, PTCs showed preserved structure (thickness), differentiation (LT labeling), and function (TexasRed-ovalbumin uptake). These data implied that such cells had now become the first line for ARME, thus maximally exposed to uptake of disulfide-rich proteins, and were predicted to be the next to suffer.

Apical Structural and Functional PTC Dedifferentiation in *Ctns*$^{-/-}$ Mice Is Asynchronous

Because megalin immunofluorescence appeared unequal among adjacent *Ctns*$^{-/-}$ PTCs along with crystal deposits (Figure 2C) and lysosomal changes (Figure 3, B–D), we compared megalin/cubilin expression in individual PTCs at 6 months to focus on early dedifferentiation. A significant fraction of megalin-expressing cells had lost detectable cubilin, but the converse was never found (Figure 8A). This finding prompted a systematic immunofluorescence analysis of apical differentiation using markers for brush border (ezrin), apical endocytic apparatus (LT-lectin), and

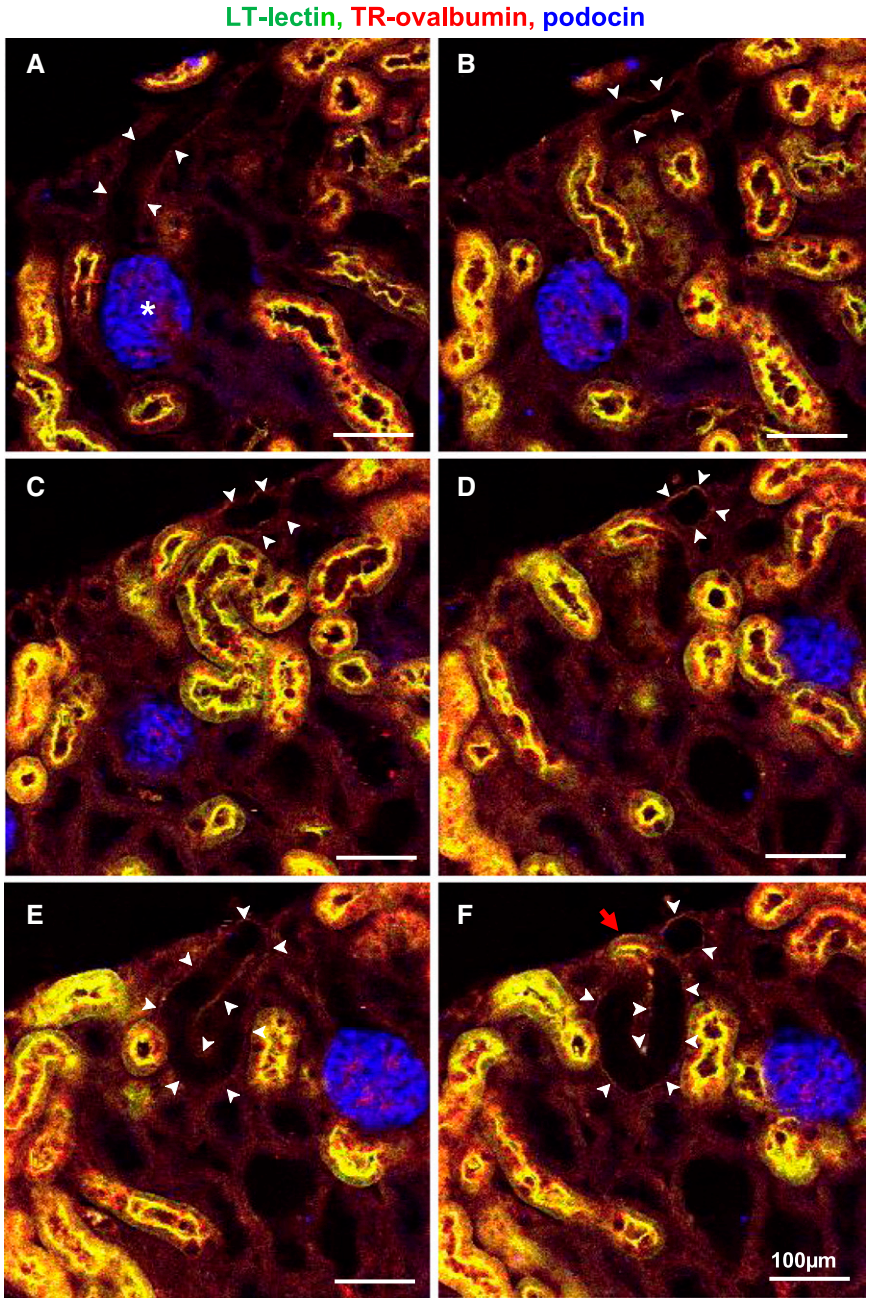

Figure 7. Longitudinal extension of swan-neck lesions in individual nephrons starting from the glomerulotubular junction can be visualized by multiphoton microscopy after multiplex fluorescence labeling. *Ctns*$^{-/-}$ mice were injected at 9 months with 600 μg TR-ovalbumin (red) like shown in Fig 6. Thick kidney slices were labeled for podocin (glomeruli; blue) and LT-lectin (PTCs; green) and resolved by serial optical sectioning over 120-μm thickness by multiphoton microscopy using 0.37-μm increments. Yellow signal indicates combined lectin labeling and ovalbumin uptake. Representative optical sections: (A) 0 μm (start level in the series), (B) 11 μm, (C) 28 μm, (D) 39 μm, (E) 53 μm, and (F) then back to 47 μm to accommodate convolution (follow proximal tubule defect for a length of >300 μm from the glomerulus). In A, PTCs (arrowheads) emerging from the glomerulus (asterisk) have completely lost lectin labeling and TR-ovalbumin uptake. In B–E, extension of swan-neck defect can be appreciated in the serial optical sections. In F, abrupt reappearance of lectin labeling coincides with TR-ovalbumin uptake (red arrow). We suggest that these cells, now first-line competent for ARME, have, thus, become most exposed to uptake of ultrafiltrated plasma proteins.

transporters relevant for Fanconi syndrome: SGLT-2 type IIa sodium-dependant phosphate cotransporter (NaPi-IIa) (Supplemental Figure 3A shows global expression level). All markers labeled WT PTC apices (Figure 8B). In *Ctns*$^{-/-}$ mice, ezrin and LT-lectin labeling selectively vanished where megalin was lost, suggesting global dedifferentiation. However, earlier loss of NaPi-IIa and cubilin over megalin (Figure 8B, d) indicated asynchronous progression into dedifferentiation.

PTC Injury Triggers Apoptosis and Epithelial Proliferation

We finally addressed whether, as reported in cultured cells,[33] cystinosis triggered PTC apoptosis, a possible mechanism for crystal clearance, and if apoptotic loss could be corrected by epithelial proliferation. Apoptosis, monitored by activated caspase-3 immunofluorescence, was hardly detected in control kidneys but easy to find in *Ctns*$^{-/-}$ PTCs after 6 months (Figure 9A, a and b). Apoptosis led to lumen shedding (Figure 9A, c and d) and was linked to PTC proliferation assessed by Ki67 immunolabeling both spatially (Figure 9A, b–d and f) and proportionally (Figure 9B, c). The highly significant correlation between apoptosis and proliferation in individual affected mice (6–12 months) also supported functional coupling (*i.e.*, epithelial regeneration and tissue repair).

DISCUSSION

Ctns$^{-/-}$ Mice Provide a Pure Model of Tubulopathy

C56BL/6 *Ctns*$^{-/-}$ mice reproduce multiple features of cystinotic nephropathy and allow us to dissect its time course. Similar urinary and PTC alterations between cystinotic mice and children indicate that defective ARME is also relevant for human cystinotic nephropathy, but preserved glomerular ultrastructure and IgG urinary absence in *Ctns*$^{-/-}$ mice up to 9 months old suggest a pure model of early tubulopathy, unlike end stage human cystinotic kidneys, which show glomerular lesions[34] and frequent glomerulotubular disconnection.[35,36] This study yielded three main findings that are likely interconnected and relevant to

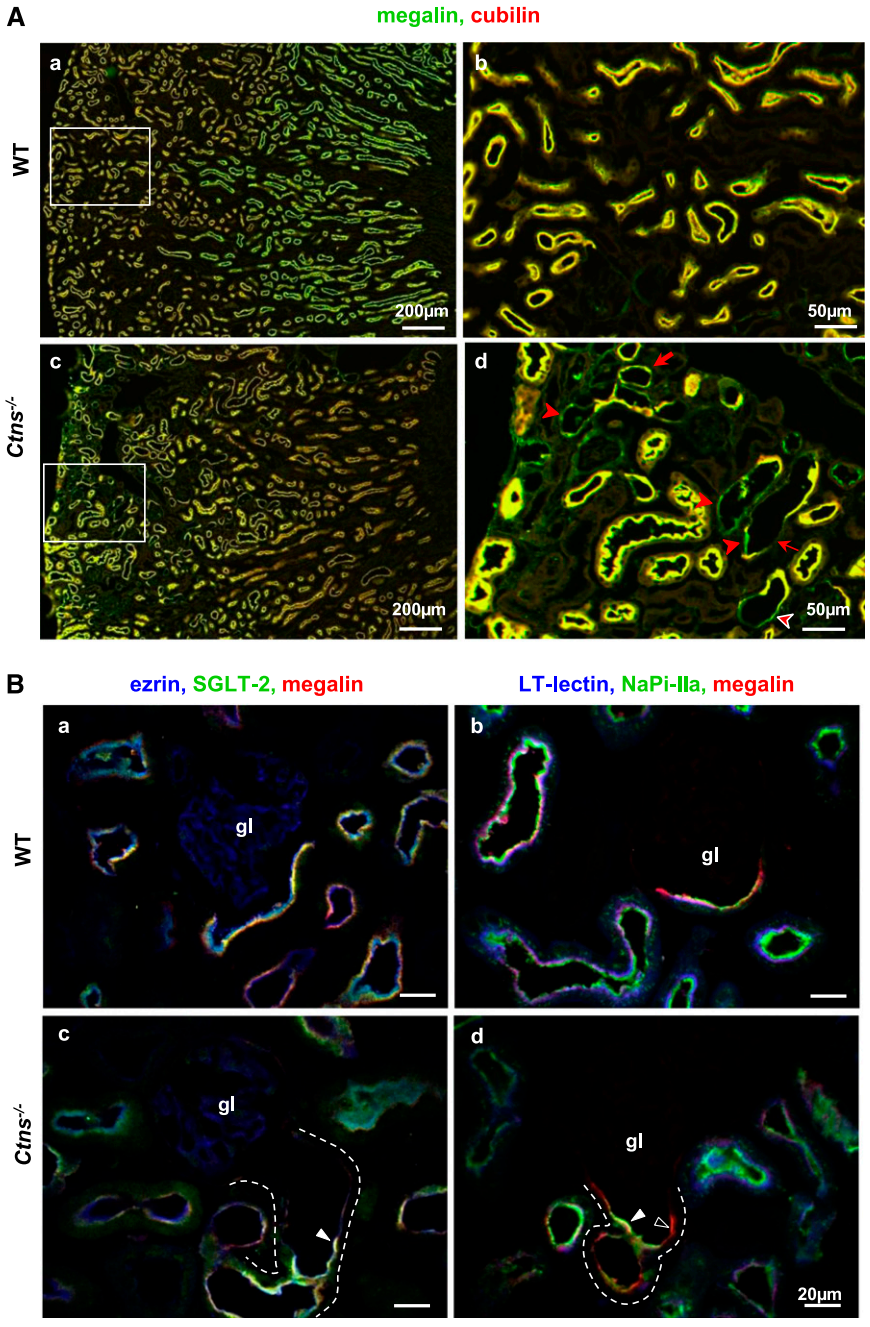

Figure 8. Multiplex immunofluorescence reveals cell-autonomous asynchronous loss of apical endocytic receptors and transporters in *Ctns*$^{-/-}$ mice cortical lesions. (A) Asynchronous loss of endocytic receptors. Paired immunofluorescence for megalin (green) and cubilin (red) in 9-month (a and b) WT and (c and d) *Ctns*$^{-/-}$ mouse kidneys. Boxed areas in a and c are enlarged in b and d. In WT mice, combined uniform expression of megalin and cubilin in the cortex generates a homogenous yellow-to-orange signal. In *Ctns*$^{-/-}$ mice, expression of both receptors is altered in cortical foci. In the enlargement shown at d, notice a triple lesional pattern/stage: (*1*) cells have a thinner apical yellow layer, indicating overall preservation of both receptors in a less-developed brush border and apical cytoplasm (thick arrow); (*2*) cells have an even thinner and only green signal, indicating additionally decreased megalin abundance and loss of detectable cubilin (arrowheads); and (*3*) PTCs do not have detectable fluorescent signal, indicating more advanced combined dedifferentiation (thin arrow). (B) Global apical PTC dedifferentiation in *Ctns*$^{-/-}$ mice cortex. Triple (immuno)fluorescence in 6-month (a and b) WT and (c and d) *Ctns*$^{-/-}$ mouse kidneys. (a and c) Combined immunolabeling for the brush border marker ezrin (blue), the sodium/glucose symporter SGLT-2 (green), and megalin (red). (b and d) Combined labeling by LT-lectin (blue) and immunolabeling for the sodium/phosphate symporter NaPi-IIa (green) and megalin (red). Note asynchronous, cell-autonomous decreased signal for LT-lectin, NaPi-IIa, SGLT-2, ezrin, and megalin in altered proximal tubules with, for example, preferential loss of NaPi-IIa over megalin (open arrowhead) adjacent to cells with combined decreased immunolabeling of megalin and NaPi-IIa or SGLT-2 (filled arrowheads). Scale bars, 20 μm.

early disease progression mechanisms: (*1*) lysosomal inclusions are concomitant with apical PTC dedifferentiation and precede crystals, (*2*) dedifferentiation likely explains the Fanconi syndrome and precedes swan-neck atrophy, and (*3*) adaptation mechanisms include cystine luminal discharge (*e.g.*, by apoptotic shedding) and proliferative epithelial repair.

Progression of the Lysosomal Cystine Form and Implications for Storage

Ctns$^{-/-}$ PTCs first show amorphous lysosomal inclusions like in human cystinotic neutrophils, where cystine is essentially soluble.[6,7] Like cystinotic fibroblasts, which actively generate but poorly retain (approximately 1%) free soluble cysteine continuously discharged by exocytosis,[10–12] PTCs in *Ctns*$^{-/-}$ kidneys incompletely retain cystine generated in lysosomes from recaptured albumin (calculations not shown). In various noncrystalline lysosome storage diseases, lysosomal expansion impacts gene expression by the transcription factor, transcription factor EB,[37] which triggers lysosomal discharge.[15] Among candidate genes promoting lysosomal discharge are Rab27a and related machineries.[38]

Amorphous inclusions are then converted into membrane-bound micrometric crystals that coalesce into huge aggregates, deforming the membrane of lysosomes and becoming progressively excluded from endocytic trafficking (*i.e.*, residual bodies). Distorted lysosomes can discharge their

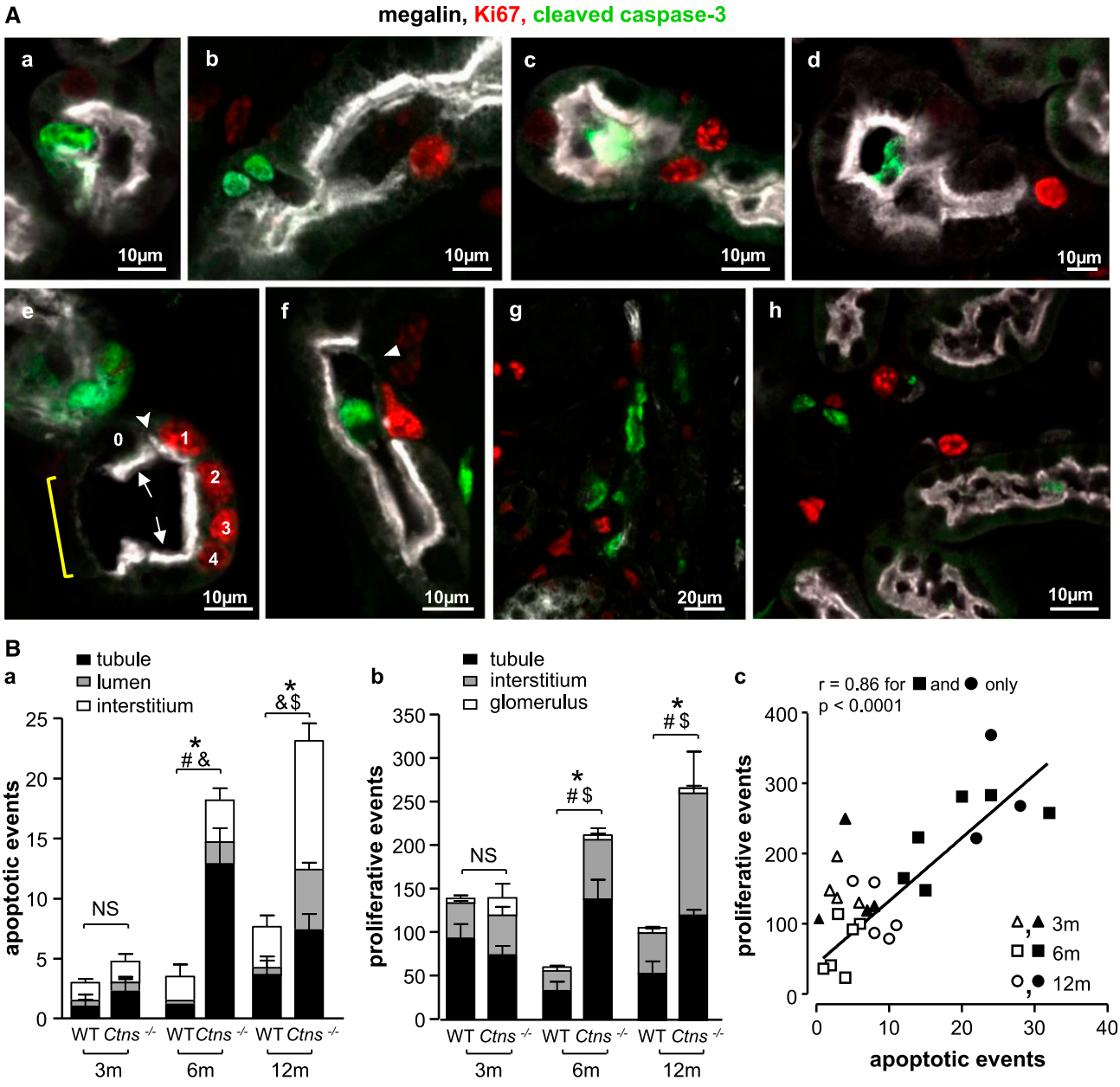

Figure 9. Apoptosis and proliferation are coordinately induced in *Ctns*$^{-/-}$ mice. (A) Triple immunofluorescence for megalin (used here as a PTC marker; white), cleaved caspase-3 (apoptotic marker; green) and Ki67 (proliferation marker; red) in (a, c, f, and g) 6- and (b, d, e, and h) 12-month *Ctns*$^{-/-}$ kidneys. This gallery compiles the following events. (*1*) Protrusion of apoptotic PTCs into the lumen (b) coupled or (a) not with proliferation within the same tubule in the same section plane. (*2*) Shedding of (c and d) apoptotic bodies into a proximal tubule lumen associated with PTC proliferation in the same tubular section. (*3*) Coexistence of (e and f) apoptosis, epithelial flattening, and proliferation. In e, a cluster of four proliferative cells (red nuclei; numbered 1–4) is separated by cells with normal height and megalin labeling (small arrows) from flattened cells with barely detectable megalin (yellow bracket); notice the discontinuity between thinner megalin labeling in proliferating cell 1 and the thicker megalin layer in the adjacent preserved cell 0 (arrowhead). In f, the uniform thick megalin layer is interrupted in the upper right (arrowhead), where a proliferative cell with red nucleus faces an apoptotic body in the lumen (green). (*4*) Extensive apoptosis and proliferation in a strongly remodeled tissue (in g, notice minimal megalin labeling above and below). (*5*) Interstitial apoptosis and proliferation between preserved PTCs (all with megalin labeling). This finding might suggest intense dynamics of the interstitial infiltrate. (B) Quantification of (a) proliferation and (b) apoptosis in 3-, 6-, and 12-month WT and *Ctns*$^{-/-}$ mouse kidneys. Cells immunolabeled for the apoptotic marker (activated/cleaved caspase-3) and the proliferation marker (Ki67) were counted in kidney sections at 3 (n=4 WT, n=4 *Ctns*$^{-/-}$), 6 (n=6 WT, n=6 *Ctns*$^{-/-}$), and 12 months (n=5 WT, n=3 *Ctns*$^{-/-}$). For each mouse, labeled cells were counted over a 2.98-mm^2 section area, corresponding to five random cortical fields. Notice significant increases of apoptosis and proliferation in 6- and 12-month-old mouse kidneys. *P<0.05 for comparison with

content by apical membrane fusion (*i.e.*, lysosomal defecation[39]) (ref.[40], figure 15). Cystine crystals are also discharged by apoptotic shedding. Although urinalysis revealed a 3- to 4-fold increase of total daily urinary cystine in *Ctns*$^{-/-}$ mice,[5] we cannot reliably quantitate the contribution of discharge as crystals, because they can dissolve in neutral urine, after which free cystine is normally recaptured by the nephron. Of note, cystinotic macrophages and corneal cells have no opportunity for luminal discharge, likely explaining the faster liver and spleen storage and early corneal crystals in patients and knockout mice.[1,41] Switching from soluble to crystalline cystine storage in cystinotic PTCs and their unique access to luminal discharge have important implications for the clock of disease progression as well as the explanation of the Fanconi syndrome, which is discussed below.

Explanation of Fanconi Syndrome and Swan-Neck Lesions

In human cystinosis, Fanconi syndrome has been attributed to PTC atrophy and is manifested as swan-neck deformities.[17] However, *Ctns*$^{-/-}$ mice reveal a clear discrepancy in timing: urinalysis narrows down the onset of the Fanconi syndrome at 3–6 months (*i.e.*, before PTC atrophy). Instead, we show an earlier loss of expression of megalin/cubilin, SGLT-2, and NaPi-IIa, which together provide a straightforward molecular explanation of proteinuria, glucosuria, and phosphaturia. Dedifferentiation before atrophy implies reversal of the apical differentiation program and might account for asynchrony between individual apical components as reported in cultured PTCs.[18] Long considered as degradative organelles, lysosomes emerge as signaling compartments that are able to impact on gene expression.[37] The signaling and transcriptional linkages between lysosomal expansion before crystals and repressed apical differentiation before atrophy deserve additional studies.

PTC atrophy, thus, develops later in *Ctns*$^{-/-}$ mice, starting at the glomerulotubular junction and extending longitudinally into typical swan-neck lesions, such as seen in cystinotic children (Figures 2B and 7).[5] What links dedifferentiation with atrophy? What accounts for longitudinal extension of swan-neck deformities? Atrophy may be considered as an ultimate stage of dedifferentiation and likely also involves autophagy, which is not addressed in this study. What we document, however, is defective apical endocytosis in S1 cells that not only leads to proteinuria but also, displaces endocytic load of disulfide-rich proteins into farther PTCs (S3). Whether distal transfer of harmful cystine load is sufficient to cause longitudinal disease progression is currently under investigation.

Another nonmutually exclusive explanation for swan-neck lesions is metaplasia by extension from Bowman's squamous epithelium into S1. This mechanism would also account for (*1*) the disappearance of PTCs normally enclosed within the Bowman's capsule of the mouse (compare Figure 2A with Figure 2B), (*2*) the much thicker basement membrane in flattened cells at swan-neck compared with normal PTCs that is similar to Bowman's capsule, and (*3*) their apparent lack of cystine crystals.

Adaptation by Cystine Disposal and Repair of Apoptosis by Epithelial Proliferation

Three potential mechanisms could account for cystine disposal: (*1*) continuous exocytosis of soluble cysteine that is able to traverse tiny tubular endosomes,[13] (*2*) later crystal exocytosis by active lysosomal defecation,[39] and (*3*) apoptotic crystal shedding. Apoptotic luminal shedding, a known mechanism of lysosomal clearance in gentamicin-induced phospholipidosis,[42] is, of course, a one-shot discharge, but it is also a trigger for epithelial proliferation. Our quantitative time course study shows increased apoptosis in 6- to 12-month-old *Ctns*$^{-/-}$ kidneys, which was reported *in vitro* based on acute cystine loading of normal cells or depletion by cysteamine of human cystinotic fibroblasts.[33] Moreover, correlation between apoptosis and PTC proliferation indicates functional coupling. Epithelial proliferation not only helps protect PTC mass and repair epithelial continuity but also, replenishes dividing cells with fresh lysosomes during the G1 phase, which may also slow down disease progression.

CONCISE METHODS

Reagents

Primers, markers, and tracers are shown in Supplemental Tables 1 and 2.

Tissues

Mouse kidneys were perfusion-fixed with 4% formaldehyde, paraffin-embedded or sucrose-infused, and frozen. Archived biopsies of four

age-matched WT for all events; $^{\#}P<0.05$ for tubular events; $^{\&}P<0.05$ for luminal events; $^{\$}P<0.05$ for interstitial events. An approximately 10-fold higher frequency for Ki67 immunolabeling compared with cleaved caspase-3 is expected, because Ki67 is expressed throughout the cell division cycle (approximately 20–24 hours), whereas apoptosis is a short event, thus with much lower probability to capture. In c, notice limited apoptosis in WT (open symbols) and 3-month *Ctns*$^{-/-}$ mice (filled triangles). In contrast, notice the strong, highly significant correlation between apoptosis and proliferation in *Ctns*$^{-/-}$ mice at 6 and 12 months (filled squares and circles), which suggests that these two events are coupled. Adaptation repair is also suggested by full preservation of relative kidney weight up to 9 months (8.46±0.27 versus 8.53±0.35 mg wet kidney/g body weight in WT versus knockout, mean±SEM, n=20 in each group, P=NS by t test; at 12 months, 8.68±0.37 versus 7.73±0.36 mg wet kidney/g body weight in WT versus knockout, mean±SEM, n=7 in each group, P=0.11, P=NS by t test).

cystinotic children and one described case[29] were compared with control human kidney.

Urinalysis

Daily (mice) or morning urine samples (from five other cystinotic children and age-matched healthy controls) (Supplemental Table 3) were analyzed for volume, glucose (glucose oxidase), inorganic phosphate,[43] proteins (Western blotting), and β-hexosaminidase.[28]

Morphology

Electron microscopy,[44] immunoperoxidase,[45] uptake of ultrafiltrated HRP (immunofluorescence), TexasRed-ovalbumin,[46] and ^{125}I-β_2-microglobulin,[27,32] multiplex (immuno)fluorescence on 5-μm frozen sections, and whole-mount (immuno)fluorescence on 200-μm vibratome slices[47] were as described or slightly modified.

RT-PCR and *In Situ* Hybridization

Quantitative RT-PCR and *in situ* hybridization on 8-μm paraffin sections were completed as described.[45,48]

Statistical Analyses

Values are means±SEMs (bar histograms) or means of individual symbols (significance of differences tested by *t* or Mann–Whitney test, respectively).

ACKNOWLEDGMENTS

We thank the biolibrary of the Université Catholique de Louvain for providing renal tissue of cystinotic and control patients, Dr. M.C. Gubler (Necker) for collecting old cystinotic kidney blocs and generously providing advice, Dr. A. Bernard and Mr. X. Dumont for performing CC16 immunoassays, Dr. E. Van Schaftingen and Mrs G. Noel for assays of glucosuria and phosphaturia, Dr. N. Van Baren for generous help in high-content imaging and reporting, L. Thanh for electron microscopy and autoradiography, and Y. Abid and S. Godecharles for assistance in morphometry.

This work was mainly supported by the Cystinosis Research Foundation, European Union Seventh Programme (EuNefron; E.L., S.C., C.A., and P.J.C.) and Belgian Science Policy Office—Interuniversity Attraction Poles Programme IAP P7/43-BeMGI. It was also supported by the Belgian Fonds de la Recherche Scientifique (FRS-FNRS) and Actions de Recherche Concertées (C.E.P. and P.J.C.) and National Institutes of Health Grants R01-DK090058 (to S.C.) and R21-DK090548 (to S.C.). The Platform for Imaging Cells and Tissues was financed by National Lottery, Région bruxelloise, Région wallonne, Université Catholique de Louvain and de Duve Institute (P.J.C.). H.P.G.C. is a Postdoctoral Researcher and C.E.P. is a Senior Research Associate at FRS-FNRS.

DISCLOSURES

None.

REFERENCES

1. Gahl WA, Thoene JG, Schneider JA: Cystinosis. *N Engl J Med* 347: 111–121, 2002
2. Nesterova G, Gahl WA: Cystinosis: The evolution of a treatable disease. *Pediatr Nephrol* 28: 51–59, 2013
3. Kalatzis V, Cherqui S, Antignac C, Gasnier B: Cystinosin, the protein defective in cystinosis, is a H(+)-driven lysosomal cystine transporter. *EMBO J* 20: 5940–5949, 2001
4. Kalatzis V, Nevo N, Cherqui S, Gasnier B, Antignac C: Molecular pathogenesis of cystinosis: Effect of CTNS mutations on the transport activity and subcellular localization of cystinosin. *Hum Mol Genet* 13: 1361–1371, 2004
5. Nevo N, Chol M, Bailleux A, Kalatzis V, Morisset L, Devuyst O, Gubler MC, Antignac C: Renal phenotype of the cystinosis mouse model is dependent upon genetic background. *Nephrol Dial Transplant* 25: 1059–1066, 2010
6. Schulman JD, Bradley KH, Seegmiller JE: Cystine: Compartmentalization within lysosomes in cystinotic leukocytes. *Science* 166: 1152–1154, 1969
7. Hummeler K, Zajac BA, Genel M, Holtzapple PG, Segal S: Human cystinosis: Intracellular deposition of cystine. *Science* 168: 859–860, 1970
8. Oude Elferink RP, Harms E, Strijland A, Tager JM: The intralysosomal pH in cultured human skin fibroblasts in relation to cystine accumulation in patients with cystinosis. *Biochem Biophys Res Commun* 116: 154–161, 1983
9. Thoene JG, Oshima RG, Ritchie DG, Schneider JA: Cystinotic fibroblasts accumulate cystine from intracellular protein degradation. *Proc Natl Acad Sci U S A* 74: 4505–4507, 1977
10. Thoene JG, Lemons R: Modulation of the intracellular cystine content of cystinotic fibroblasts by extracellular albumin. *Pediatr Res* 14: 785–787, 1980
11. Thoene JG, Lemons RM: Cystine accumulation in cystinotic fibroblasts from free and protein-linked cystine but not cysteine. *Biochem J* 208: 823–830, 1982
12. Pisoni RL, Acker TL, Lisowski KM, Lemons RM, Thoene JG: A cysteine-specific lysosomal transport system provides a major route for the delivery of thiol to human fibroblast lysosomes: Possible role in supporting lysosomal proteolysis. *J Cell Biol* 110: 327–335, 1990
13. Christensen EI: Rapid membrane recycling in renal proximal tubule cells. *Eur J Cell Biol* 29: 43–49, 1982
14. Carpentier S, N'Kuli F, Grieco G, Van Der Smissen P, Janssens V, Emonard H, Bilanges B, Vanhaesebroeck B, Gaide Chevronnay HP, Pierreux CE, Tyteca D, Courtoy PJ: Class III phosphoinositide 3-kinase/VPS34 and dynamin are critical for apical endocytic recycling. *Traffic* 14: 933–948, 2013
15. Medina DL, Fraldi A, Bouche V, Annunziata F, Mansueto G, Spampanato C, Puri C, Pignata A, Martina JA, Sardiello M, Palmieri M, Polishchuk R, Puertollano R, Ballabio A: Transcriptional activation of lysosomal exocytosis promotes cellular clearance. *Dev Cell* 21: 421–430, 2011
16. Christensen EI, Wagner CA, Kaissling B: Uriniferous tubule: Structural and functional organization. *Compr Physiol* 2: 805–861, 2012
17. Mahoney CP, Striker GE: Early development of the renal lesions in infantile cystinosis. *Pediatr Nephrol* 15: 50–56, 2000
18. Lima WR, Parreira KS, Devuyst O, Caplanusi A, N'kuli F, Marien B, Van Der Smissen P, Alves PM, Verroust P, Christensen EI, Terzi F, Matter K, Balda MS, Pierreux CE, Courtoy PJ: ZONAB promotes proliferation and represses differentiation of proximal tubule epithelial cells. *J Am Soc Nephrol* 21: 478–488, 2010
19. Toledano MB, Delaunay-Moisan A, Outten CE, Igbaria A: Functions and cellular compartmentation of the thioredoxin and glutathione pathways in yeast. *Antioxid Redox Signal* 18: 1699–1711, 2013

20. Christensen EI, Verroust PJ: Megalin and cubilin, role in proximal tubule function and during development. *Pediatr Nephrol* 17: 993–999, 2002
21. Pfeifer U, Scheller H: A morphometric study of cellular autophagy including diurnal variations in kidney tubules of normal rats. *J Cell Biol* 64: 608–621, 1975
22. Christensen EI, Birn H: Megalin and cubilin: Multifunctional endocytic receptors. *Nat Rev Mol Cell Biol* 3: 256–266, 2002
23. Leheste JR, Rolinski B, Vorum H, Hilpert J, Nykjaer A, Jacobsen C, Aucouturier P, Moskaug JO, Otto A, Christensen EI, Willnow TE: Megalin knockout mice as an animal model of low molecular weight proteinuria. *Am J Pathol* 155: 1361–1370, 1999
24. Weyer K, Storm T, Shan J, Vainio S, Kozyraki R, Verroust PJ, Christensen EI, Nielsen R: Mouse model of proximal tubule endocytic dysfunction. *Nephrol Dial Transplant* 26: 3446–3451, 2011
25. Weyer K, Nielsen R, Christensen EI, Birn H: Generation of urinary albumin fragments does not require proximal tubular uptake. *J Am Soc Nephrol* 23: 591–596, 2012
26. Amsellem S, Gburek J, Hamard G, Nielsen R, Willnow TE, Devuyst O, Nexo E, Verroust PJ, Christensen EI, Kozyraki R: Cubilin is essential for albumin reabsorption in the renal proximal tubule. *J Am Soc Nephrol* 21: 1859–1867, 2010
27. Christensen EI, Devuyst O, Dom G, Nielsen R, Van der Smissen P, Verroust P, Leruth M, Guggino WB, Courtoy PJ: Loss of chloride channel ClC-5 impairs endocytosis by defective trafficking of megalin and cubilin in kidney proximal tubules. *Proc Natl Acad Sci U S A* 100: 8472–8477, 2003
28. Nielsen R, Courtoy PJ, Jacobsen C, Dom G, Lima WR, Jadot M, Willnow TE, Devuyst O, Christensen EI: Endocytosis provides a major alternative pathway for lysosomal biogenesis in kidney proximal tubular cells. *Proc Natl Acad Sci U S A* 104: 5407–5412, 2007
29. Wilmer MJ, Christensen EI, van den Heuvel LP, Monnens LA, Levtchenko EN: Urinary protein excretion pattern and renal expression of megalin and cubilin in nephropathic cystinosis. *Am J Kidney Dis* 51: 893–903, 2008
30. Zhai XY, Birn H, Jensen KB, Thomsen JS, Andreasen A, Christensen EI: Digital three-dimensional reconstruction and ultrastructure of the mouse proximal tubule. *J Am Soc Nephrol* 14: 611–619, 2003
31. Straus W: Cytochemical observations on the relationship between lysosomes and phagosomes in kidney and liver by combined staining for acid phosphatase and intravenously injected horseradish peroxidase. *J Cell Biol* 20: 497–507, 1964
32. Jouret F, Walrand S, Parreira KS, Courtoy PJ, Pauwels S, Devuyst O, Jamar F: Single photon emission-computed tomography (SPECT) for functional investigation of the proximal tubule in conscious mice. *Am J Physiol Renal Physiol* 298: F454–F460, 2010
33. Park M, Helip-Wooley A, Thoene J: Lysosomal cystine storage augments apoptosis in cultured human fibroblasts and renal tubular epithelial cells. *J Am Soc Nephrol* 13: 2878–2887, 2002
34. Wilmer MJ, Emma F, Levtchenko EN: The pathogenesis of cystinosis: Mechanisms beyond cystine accumulation. *Am J Physiol Renal Physiol* 299: F905–F916, 2010
35. Larsen CP, Walker PD, Thoene JG: The incidence of atubular glomeruli in nephropathic cystinosis renal biopsies. *Mol Genet Metab* 101: 417–420, 2010
36. Chevalier RL, Forbes MS: Generation and evolution of atubular glomeruli in the progression of renal disorders. *J Am Soc Nephrol* 19: 197–206, 2008
37. Sardiello M, Palmieri M, di Ronza A, Medina DL, Valenza M, Gennarino VA, Di Malta C, Donaudy F, Embrione V, Polishchuk RS, Banfi S, Parenti G, Cattaneo E, Ballabio A: A gene network regulating lysosomal biogenesis and function. *Science* 325: 473–477, 2009
38. Johnson JL, Napolitano G, Monfregola J, Rocca CJ, Cherqui S, Catz SD: Upregulation of the Rab27a-dependent trafficking and secretory mechanisms improves lysosomal transport, alleviates endoplasmic reticulum stress, and reduces lysosome overload in cystinosis. *Mol Cell Biol* 33: 2950–2962, 2013
39. De Duve C, Wattiaux R: Functions of lysosomes. *Annu Rev Physiol* 28: 435–492, 1966
40. Maunsbach AB: Observations on the ultrastructure and acid phosphatase activity of the cytoplasmic bodies in rat kidney proximal tubule cells. With a comment on their classification. *J Ultrastruct Res* 16: 197–238, 1966
41. Simpson J, Nien CJ, Flynn K, Jester B, Cherqui S, Jester J: Quantitative in vivo and ex vivo confocal microscopy analysis of corneal cystine crystals in the Ctns knockout mouse. *Mol Vis* 17: 2212–2220, 2011
42. Tulkens PM: Experimental studies on nephrotoxicity of aminoglycosides at low doses. Mechanisms and perspectives. *Am J Med* 80[Suppl 6B]: 105–114, 1986
43. Fiske CH, Subbarow Y: The colorimetric determination of phosphorus. *J Biol Chem* 66: 375–400, 1925
44. Maunsbach AB: The influence of different fixatives and fixation methods on the ultrastructure of rat kidney proximal tubule cells. I. Comparison of different perfusion fixation methods and of glutaraldehyde, formaldehyde and osmium tetroxide fixatives. *J Ultrastruct Res* 15: 242–282, 1966
45. Gaide Chevronnay HP, Cornet PB, Delvaux D, Lemoine P, Courtoy PJ, Henriet P, Marbaix E: Opposite regulation of transforming growth factors-beta2 and -beta3 expression in the human endometrium. *Endocrinology* 149: 1015–1025, 2008
46. Caplanusi A, Parreira KS, Lima WR, Marien B, Van Der Smissen P, de Diesbach P, Devuyst O, Courtoy PJ: Intravital multi-photon microscopy reveals several levels of heterogeneity in endocytic uptake by mouse renal proximal tubules. *J Cell Mol Med* 12: 351–354, 2008
47. Pierreux CE, Cordi S, Hick AC, Achouri Y, Ruiz de Almodovar C, Prévot PP, Courtoy PJ, Carmeliet P, Lemaigre FP: Epithelial: Endothelial crosstalk regulates exocrine differentiation in developing pancreas. *Dev Biol* 347: 216–227, 2010
48. Hick AC, van Eyll JM, Cordi S, Forez C, Passante L, Kohara H, Nagasawa T, Vanderhaeghen P, Courtoy PJ, Rousseau GG, Lemaigre FP, Pierreux CE: Mechanism of primitive duct formation in the pancreas and submandibular glands: A role for SDF-1. *BMC Dev Biol* 9: 66, 2009
49. Norden AG, Gardner SC, Van't Hoff W, Unwin RJ: Lysosomal enzymuria is a feature of hereditary Fanconi syndrome and is related to elevated CI-mannose-6-P-receptor excretion. *Nephrol Dial Transplant* 23: 2795–2803, 2008
50. Luzio JP, Pryor PR, Bright NA: Lysosomes: Fusion and function. *Nat Rev Mol Cell Biol* 8: 622–632, 2007

This article contains supplemental material online at http://jasn.asnjournals.org/lookup/suppl/doi:10.1681/ASN.2013060598/-/DCSupplemental.